Observations of high energy electrons in Jupiter's innermost radiation belts and polar regions by the Juno radiation monitoring investigation: Perijoves 1 and 3

Heidi N. Becker[1], Daniel Santos-Costa[2], John L. Jørgensen[3], Troelz Denver[3], Alberto Adriani[4], Alessandro Mura[4], John E.P. Connerney[5,6], Scott J. Bolton[2], Steven M. Levin[1], Richard M. Thorne[7], James W. Alexander[1], Virgil Adumitroaie[1], Emily A. Manor-Chapman[1], Ingrid J. Daubar[1], Clifford Lee[1], Mathias Benn[3], Julia Sushkova[3], Andrea Cicchetti[4], Raffaella Noschese[4]

[1]Jet Propulsion Laboratory, California Institute of Technology, 4800 Oak Grove Drive, Pasadena, CA 91109, U.S.A.

[2]Southwest Research Institute, San Antonio, TX, United States.

[3]DTU Space, National Space Institute, Technical University of Denmark, Kgs Lyngby, Denmark.

[4]INAF, Istituto di Astrofisica e Planetologia Spaziali, Rome, Italy.

[5]Space Research Corporation, Annapolis, MD, United States.

[6]NASA Goddard Space Flight Center, Greenbelt, MD, United States.

[7]UCLA, Department of Atmospheric and Oceanic Sciences, Los Angeles, CA 90095.

Corresponding author: Heidi N. Becker (Heidi.N.Becker@jpl.nasa.gov)

High latitude sampling of relativistic electrons at inner edge of Jovian radiation belts

Abstract

Juno's "Perijove 1" (August 27, 2016) and "Perijove 3" (December 11, 2016) flybys through the innermost region of Jupiter's magnetosphere (1.06 Jovian radii at closest approach) provided the first look at Jupiter's innermost radiation environment. The Juno Radiation Monitoring Investigation collected particle counts and noise signatures from penetrating high energy particle impacts in images acquired by the Stellar Reference Unit and Advanced Stellar Compass star trackers and the JIRAM infrared imager. This coordinated observation campaign sampled radiation at the inner edges of the high latitude lobes of the synchrotron emission region as well as more distant environments. The inferred omnidirectional >5 MeV and >10 MeV electron fluxes derived from these measurements will provide valuable constraints for models of relativistic electron environments in the innermost radiation belts. Several intense bursts of high-energy particle counts were also observed by the Advanced Stellar Compass in both polar regions.

1 Introduction

Jupiter's inner magnetosphere is largely unexplored. Our understanding of the relativistic electron population within the innermost radiation belts has been guided by remote observation of synchrotron emission and in situ measurements obtained during two prior missions. Pioneer 11 provided energetic particle counts during its high inclination flyby, passing to within ~1.6 Rj of Jupiter in 1974 (-13° latitude at closest approach), and the Galileo probe sampled energetic particles along its approximately equatorial trajectory into Jupiter's atmosphere in 1995 [*Bolton et al.*, 2004; *Fischer et al.*, 1996]. However, these two encounters provide limited coverage of this complex environment. Juno's unprecedented polar orbit enables data collection at high magnetic latitudes, through the inner edges of the high latitude lobes of the synchrotron region (a region inside ~3.5 Rj where synchrotron emission from relativistic electrons contributes to the Jovian radio emission [*Carr et al.*, 1983]), and to within 1.06 Rj at periapsis (Figure 1). Juno's 32 planned science orbits with ~12° longitude separation will provide extensive sampling of energetic particles within Jupiter's innermost radiation belts and polar regions.

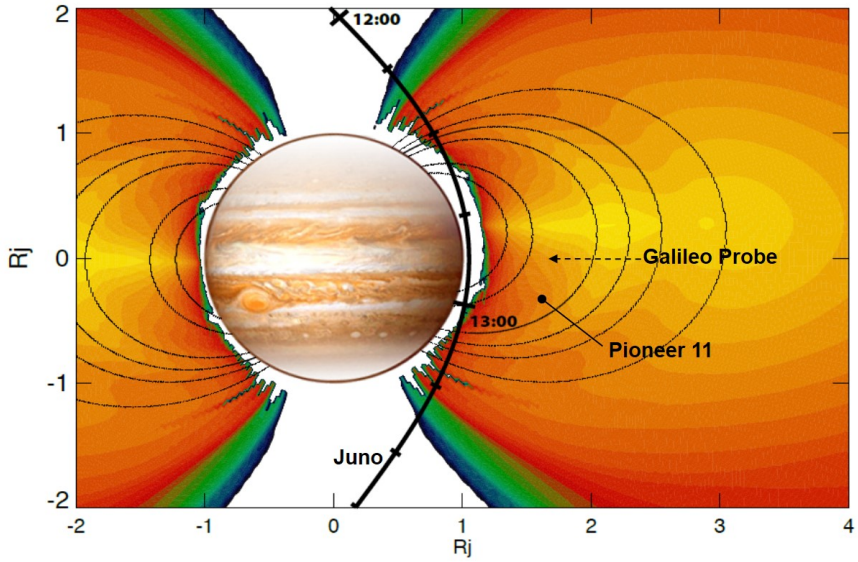

Figure 1. Juno's "Perijove 1" trajectory through the inner magnetosphere on August 27, 2016. Times shown along the black trajectory curve are given in UTC with tick marks at 15 minute intervals. The spacecraft range was 1.06 Rj (4,147 km from the cloud tops) at closest approach; 12:50:44 UTC. The flyby provided a first look at territory not sampled by in-situ high energy particle instrumentation during past missions. Markers indicate the range of the Pioneer 11 spacecraft at its closest approach to the planet, and the path of the Galileo Probe into Jupiter's atmosphere.

Juno's Radiation Monitoring (RM) Investigation acquires profiles of Jupiter's >10-MeV electron environment within unexplored regions of the Jovian magnetosphere using a novel measurement approach. The detectors inside Juno's heavily shielded instruments register impacts from penetrating charged particles (particles with enough energy to traverse the heavily shielded instrument enclosures). Particle impacts upon sensitive focal plane arrays result in elevated noise signals within clusters of pixels proximate to the ionization events created by the particle "hits." RM actively retrieves this noise in collaborative observation campaigns of "radiation image" and penetrating particle count collection at targeted locations within the magnetosphere during each of Juno's perijove passes. Instruments contributing to the campaign include the spacecraft Stellar Reference Unit (SRU), the Magnetic Field Investigation's Advanced Stellar Compass camera head D imager (ASC) [*Connerney et al.*, 2017], and the JIRAM infrared imager [*Adriani et al.*, 2014]. A combination of on-board and ground-based image processing is used to extract the characteristic signatures of penetrating high energy electrons (Figure 2) and derive count rates to characterize the external environment. The count rate processing algorithms were designed using knowledge of the distinctive signals and morphology of noise generated by external particles in each of these instruments. Extensive pre-flight and post-launch radiation testing, combined with Geant4 Monte Carlo analysis [*Allison*, 2006] of particle interactions within the shielded instruments, provided recognizable radiation signatures unique to each instrument [*Becker et al.*, 2016].

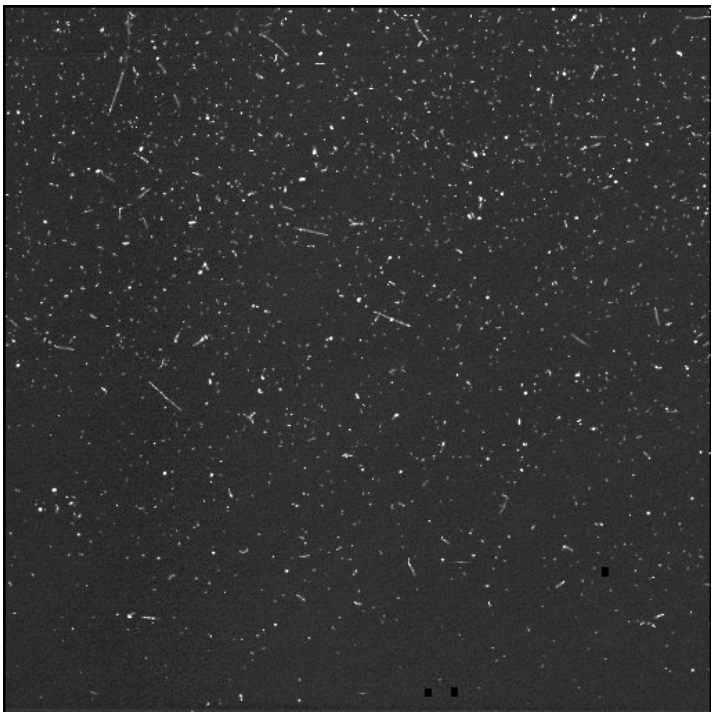

Figure 2. SRU CCD image collected at 13:18:16.336 UTC August 27, 2016 within Jupiter's inner radiation belts (1.4Rj; -54.3° dipole magnetic latitude, derived from the VIP4 model [*Connerney et al.*, 1998]). The image illustrates characteristic imager noise signatures (white) due to penetrating relativistic electrons. Three small pixel regions in the lower part of the image (black squares) were removed prior to particle count rate processing due to the presence of star signal above the particle noise detection threshold.

Geant4 shielding analysis was performed for each instrument to characterize the penetration efficiencies of omnidirectional high energy electrons as a function of their external energy (prior to entering the instrument). These probabilities were interpolated over energy and integrated using modeled Jovian environment spectra from *Garrett et al.* [2005], *Divine and Garrett* [1983], and *Garrett et al.* [2003] to assess instrument count rate response in similar environments. The external energy above which the dominant contribution to the overall count rate was made was identified in order to define an approximate energy channel and count rate metric for each instrument. This allows the external environment flux to be inferred from the count rates of noise events observed in the respective images (Table 1). Simultaneous observations gathered by the instruments provide comparative spectral information due to differing spectral sensitivities brought about by significant differences in instrument shielding.

Table 1. Approximate energy channels and measurement ranges of the Juno RM instruments. Lower energies are expected to make a relatively small contribution to the count rate in hard spectral environments. Measurement ranges apply for the nominal 1-sec JIRAM imager exposures and 125-ms single field ASC imaging.

Instrument	Energy sensitivity (electrons)	Measurement Range (count rate)	Inferred external omnidirectional flux (electrons cm^{-2} s^{-1})
SRU CCD imager	>10-MeV	4E2-1.6E7 (counts cm^{-2} CCD s^{-1})	2E4-1E9
JIRAM infrared imager	>5-MeV	4E5-1E7 (penetrating events s^{-1})	1.2E6-3E7
ASC CCD imager (on-board particle counter)	>10-MeV	600-10,000 (reported CCD impacts per image)	3E5-5E6

In this letter we discuss the first high latitude sampling of >10 MeV electrons at the innermost edge of the Jovian radiation belts and observations of high energy penetrators in Jupiter's polar regions during Juno's Perijove 1 and Perijove 3 flybys.

2 Observations

The SRU, ASC, and JIRAM imagers made coordinated measurements of the Jovian radiation environment during Juno's first science pass over the poles and through the inner magnetosphere from ~12:00 to 13:45 UTC on August 27, 2016. ASC particle count data (an on-board count of the transient radiation signatures detected within each image field) were collected at a 4 Hz sampling rate throughout the passage. Six SRU image samples were collected at targeted opportunities within the inner magnetosphere and polar regions (Figure 3a). The significantly lower SRU sampling rate is due to constraints levied by its primary engineering function, the support of spacecraft attitude determination. Fifty-one JIRAM images were collected during the observation period, including 6 coincident with SRU image collection.

Perijove 3 did not include JIRAM science observations due to a spacecraft engineering issue related to on-board JIRAM data management. SRU and ASC RM data were collected. Figure 3 shows Perijove 3 SRU imaging locations within the period of ~16:15 to 18:00 UTC on December 11, 2016. In addition to 4 Hz ASC particle count sampling, ASC images collected at the times of SRU imaging were also retrieved during Perijove 3 for SRU observation times up to and including Juno's passage through the northern high latitude lobe of the synchrotron region. Ground processing of the ASC images confirmed the count rates reported by the ASC on-board particle counting algorithms at the same sampling times.

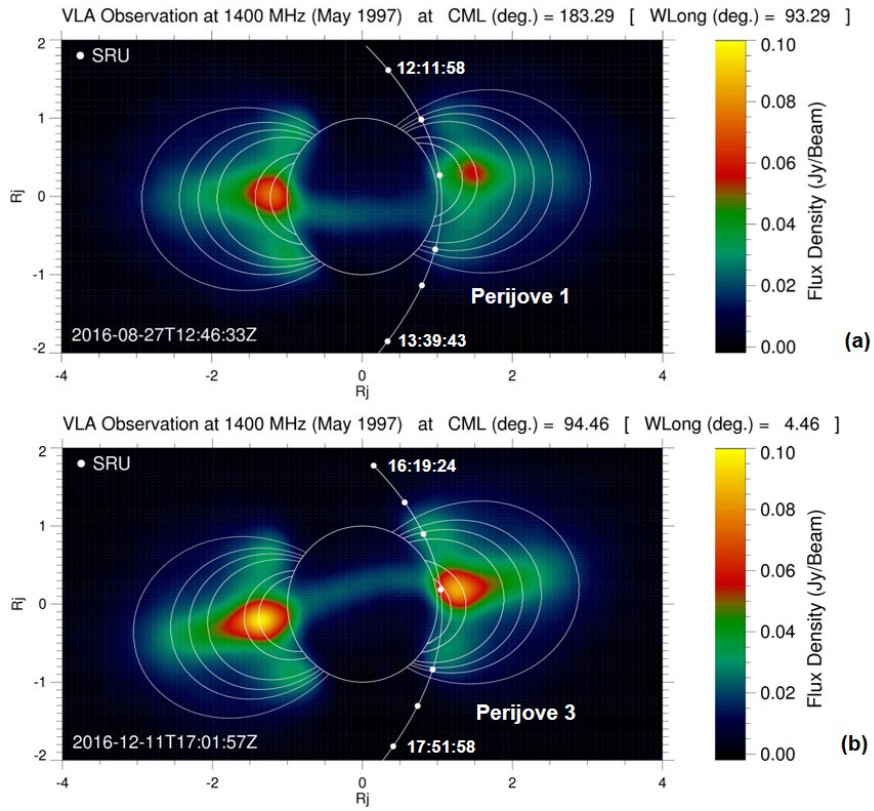

Figure 3. SRU image collection locations (white dots) along Juno's Perijove 1 (**a**) and Perijove 3 (**b**) science passes. Integrated flux density of synchrotron emission is shown (~21 cm, averaged over 20 degrees of longitude) for context. The synchrotron map projections (after *Santos-Costa et al.* [2014]) are given for the central meridian longitude corresponding to the System III West longitude of the spacecraft near the time of the magnetic equator crossing of each flyby (crossing times are shown in the lower left corners of the maps). Magnetic field lines are plotted for L=1.3, 1.5, 2, 2.25, 2.5, 3 and were calculated using the VIP4 magnetic field model [*Connerney et al.*, 1998]. SRU image collection was targeted to occur as Juno's trajectory grazed the inner edges of the high latitude lobes of the synchrotron region.

2.1 Perijove 1 Results

Figure 4a shows inferred omnidirectional >5 MeV and >10 MeV electron fluxes as a function of time derived from JIRAM, ASC, and SRU measurements collected during Perijove 1. Fluxes inferred from the three instruments are remarkably consistent. Fluxes decrease near the orbits of Io and Amalthea, and increase radially inward of each satellite's orbital radius. Similar behavior is also seen a bit more subtly near the orbit of Thebe. Similar dips and peaks were observed in the Pioneer electron flux data [*Fillius*, 1976] and Galileo probe data [*Fischer et al.*, 1996], attributed to satellite absorption (sweeping) effects [*Fillius,*1976]. ASC detected fluxes inward to a spacecraft range of 1.18Rj (dipole magnetic latitude 37.6°) at 12:35 UTC; detection resumed outbound from closest approach (CA) at 13:00 UTC (1.1Rj, dipole magnetic latitude -21.2°).

In Figure 4 we compare RM electron fluxes to omnidirectional >10 MeV electron fluxes predicted by the physical model of *Santos-Costa and Bolton* [2008] (grey curves) and the

empirical model of *Garrett et al.* [2005] (pink curves). Differences are observed between the RM flux measurements and the model predictions; the measurements were generally found to be lower than predicted fluxes within the synchrotron region. The discrepancies are largest for spacecraft locations <1.3 Rj corresponding approximately to calculated L-shells inside the orbit of Amalthea.

An intense radiation peak was observed in the ASC particle counter data at 13:35:45 UTC. It was accompanied by detection of many bright objects in the field of view of all four ASC camera heads, though not precisely at the same instant; the four ASC camera heads scan two distinct directions in the sky. This interesting event occurred as the spacecraft was transiting the southern polar region outbound from Perijove 1 (1.8Rj, -71.8° dipole magnetic latitude) and coincides with an intense, asymmetric bi-directional electron beam identified by Juno's JEDI [*Mauk et al.*, 2014] investigation at the same time [*Mauk et al.*, 2016]. JEDI investigators noted that the beam occurred near the statistical main auroral oval and appeared to be quite spectrally hard. Neither SRU nor JIRAM images were collected at this particular location; however a JIRAM image collected immediately following at 13:36:07 UTC contained penetrating particle signatures at a relatively low level, below the calibrated measurement range for JIRAM radiation measurements.

2.2 Perijove 3 Results

Figure 4b shows derived >10 MeV electron fluxes as a function of time along the trajectory from ASC particle counter measurements and SRU images collected during Perijove 3. Times during which the spacecraft traversed L-shells associated with the Jovian satellites and ring are indicated in Figure 4a, along with omnidirectional >10-MeV electron flux model predictions. As observed with Perijove 1, RM measurements during Perijove 3 indicated lower than anticipated electron fluxes in the innermost radiation belts. Similar dips in flux were observed in the vicinities of Io and Amalthea, followed by small peaks inside their respective orbits. In contrast to the model predictions, a drop off in ASC particle count detection occurred at 16:53 at a range of 1.12 Rj and a clear radiation "gap" was observed by the ASC in the equatorial region near closest approach (CA at 17:03:40; 1.06 Rj, 5.7° latitude, 5.5° SIII W longitude). This is consistent with the energetic electron flux measurements of the Galileo probe EPI instrument [*Fischer et al.*, 1996] which showed a disappearance of particles inside ~1.25 Rj at a similar SIII W longitude (4.94° W longitude, 6.53° latitude at time of probe entry according to *Bell* [1996]). The SRU image collected at 17:02:11.981 (1.06 Rj, 9.5° latitude, 4.6° SIII W longitude) confirmed the absence of high energy electron flux in this region. The ASC resumed particle detection outbound from periapsis at 17:15, at ranges >1.12 Rj.

The ASC again reported intense bursts of penetrating particle counts as Juno transited Jupiter's polar regions during the Perijove 3 flyby. Events were observed in the north at 15:40 and from ~15:54-16:17, as well as at 17:38 soon after exiting the radiation belts in the south.

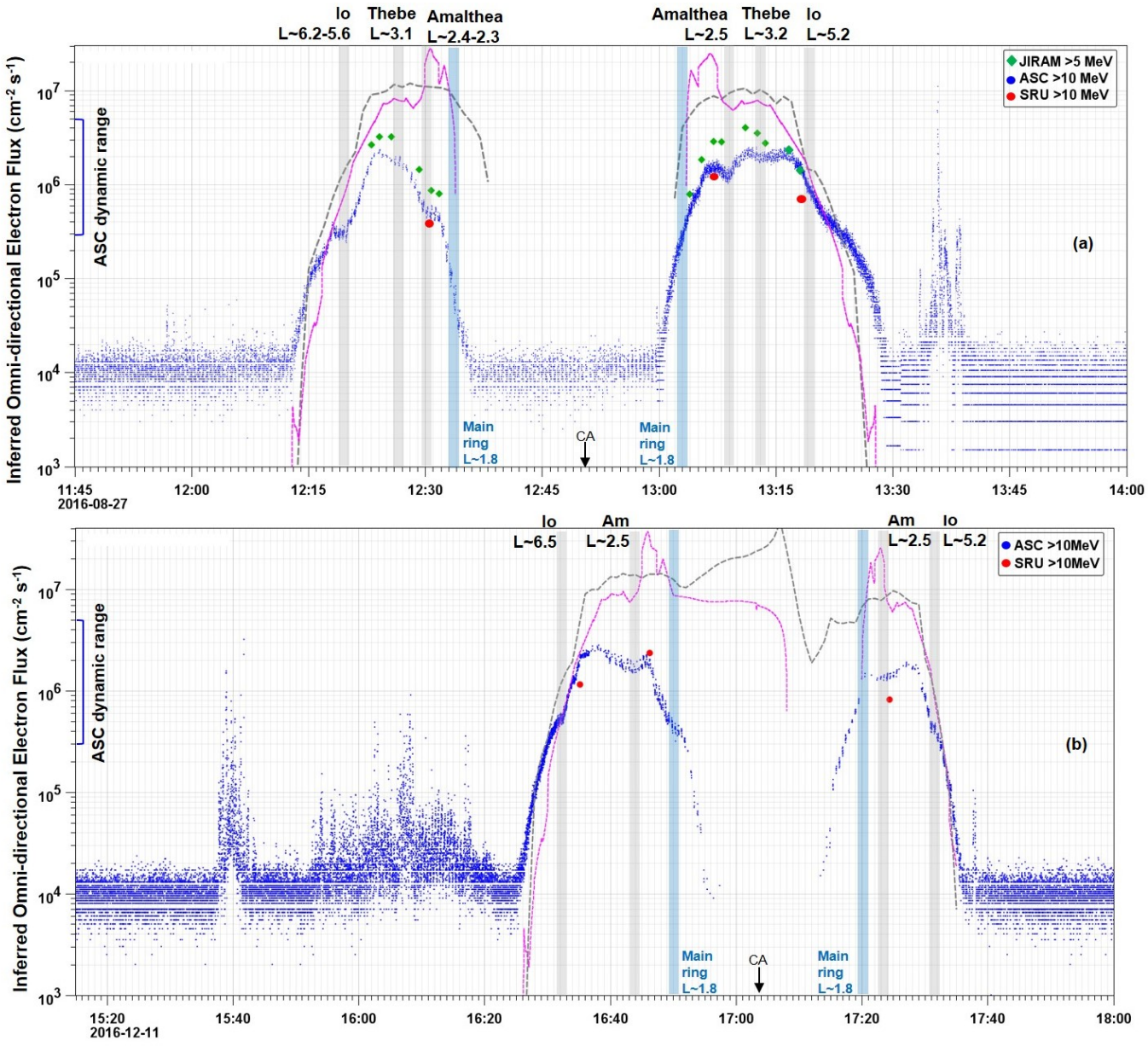

Figure 4. Omnidirectional fluxes of >5 MeV and >10MeV electrons derived from penetrating particle count rates observed by the SRU, ASC, and JIRAM imagers along Juno's Perijove 1 (**a**) and Perijove 3 (**b**) trajectories. SRU and JIRAM measurements with count rates lower than the calibrated measurement range, or zero, have been omitted from the plot. ASC data have been corrected for electronic shutter time and filtered to remove samples affected by straylight. ASC data points at ~10^4 are due to a small star field dependent bias caused by dim stars reported amongst the count of penetrators (established with data collected during Juno's Cruise period outside of the Jovian magnetosphere). Grey bars show regions of L shell (calculated using the VIP4 magnetic field model [*Connerney et al.*, 1998] and the magnetodisc model of *Connerney, Acuña, and Ness* [1981]) associated with the orbits of several Jovian moons; blue bars mark L shells associated with the main Jovian ring; closest approach is marked "CA." Omnidirectional

202 >10 MeV electron flux predictions using *Santos-Costa and Bolton* [2008] (grey dashed lines)
203 and *Garrett et al.* [2005] (pink dashed lines) with VIP4 are shown for comparison.

204

205 **3 Discussion**

206 The differences seen between the model predictions and RM's inferred >10 MeV electron
207 flux measurements suggest that RM measurements will be very beneficial in improving our
208 understanding of electron energy spectra and pitch angle distributions close to the planet. Juno is
209 the first spacecraft to encounter these regions within the inner radiation belts. Departures of the
210 measured magnetic field from VIP4 model predictions (discussed in *Bolton et al.* [2017]) may
211 also contribute to the differences as VIP4 magnetic field predictions were used in deriving the
212 modeled electron fluxes.

213 An added consideration is that the RM instruments are detecting penetrating electrons
214 from rather broad energy channels (>5 MeV and >10 MeV), and a distribution of penetration
215 efficiency energy "bins" exists within each channel (Figure 5). The fractional contribution to the
216 total count rate from a given energy bin would be expected to vary as a result of differences in
217 spectral hardness of the ambient external particle population. Simultaneous measurements by the
218 RM instruments provide the opportunity to study these higher external energies by comparing
219 the responses of the different instruments at the same sampling locations. As illustrated in Figure
220 5 the three instruments have differing sensitivities to energies above 10 MeV. The ASC count
221 rates are significantly influenced by the >20-MeV electron population within the external
222 environment, whereas the SRU exhibits a more gradual increase in sensitivity to higher energies
223 due to its very different shielding configuration. JIRAM is relatively more sensitive at energies
224 <10 MeV and provides added information about this part of the external spectra. Modeling work
225 incorporating electron flux data from the JEDI investigation (~20-1000 keV) will further guide
226 the analysis. RM measurements show great promise in aiding our understanding of Jupiter's
227 radiation belts, particularly with respect to pitch angle and energy distributions within the inner
228 edges of Jupiter's radiation belts. Measurements from Juno's ongoing longitude mapping of the
229 inner magnetosphere will also be very important to our understanding of the data. Magnetic Field
230 Investigation, JEDI, and Microwave Radiometer investigations will provide key data sets.

231 In future orbits, a greater number of SRU images will be collected near Juno's expected
232 crossings of the northern and southern auroral ovals (coordinated with JIRAM and ASC image
233 retrieval when compatible) to increase the likelihood of measuring additional energetic electron
234 beam events with multiple RM instruments. Such measurements would corroborate inferred flux
235 levels detected by the on-board ASC particle counter and provide additional insight into the
236 energy distribution at the higher energies, contributing to the further study of the energy spectra
237 of these events.

238

239

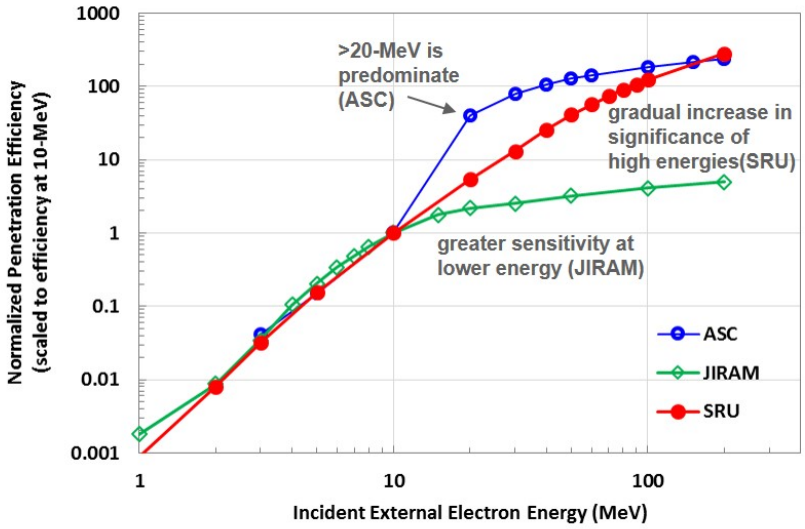

240

241 **Figure 5.** Comparison of the spectral sensitivities of the ASC, SRU, and JIRAM. The
242 probabilities of omnidirectional high energy electrons to penetrate instrument shielding and
243 create image noise events ("penetration efficiencies") have been normalized to the value at 10-
244 MeV for each instrument.

245

246 **Acknowledgments and Data**

247 We thank the larger Juno ASC, JIRAM, and Magnetic Field Investigation Teams; the Lockheed
248 Martin GN&C and Spacecraft Operations Teams; the Selex Galileo Juno SRU Team; John
249 Allison, Stephen Watts, Shawn Kang, William McAlpine, and Karen Willacy for their
250 contributions to the development of the Radiation Monitoring Investigation. This work was
251 sponsored by the Jet Propulsion Laboratory, California Institute of Technology, under a contract
252 with the National Aeronautics and Space Administration. The JIRAM Project is funded by the
253 Italian Space Agency. The data presented here currently reside at the Jet Propulsion Laboratory.
254 Inquiries regarding obtaining data may be directed to the lead author.

256 **References**

257 Adriani, A., Filacchione, G., Di Iorio, T. et al. (2014), JIRAM, the Jovian Infrared Auroral
258 Mapper, Space Sci Rev, doi:10.1007/s11214-014-0094-y.

259 Allison, J., et al. (2006), Geant4 developments and applications, IEEE Trans. Nuclear Science,
260 53(1), 270-278, doi: 10.1109/TNS.2006.869826.

261 Becker, H.N., J.W. Alexander, A. Adriani, A. Mura, A. Cicchetti, R. Noschese, J.L. Jørgensen,
262 T. Denver, J. Sushkova, A. Jørgensen, M. Benn, J.E.P. Connerney, S.J. Bolton, the Selex
263 Galileo Juno SRU Team, J. Allison, S. Watts, V. Adumitroaie, E.A. Manor-Chapman, I.J.
264 Daubar, C. Lee, S. Kang, W.J. McAlpine, T. Di Iorio, C. Pasqui, A. Barbis, P. Lawton, L.

265 Spalsbury, S. Loftin, and J. Sun (2017), The Juno Radiation Monitoring (RM)
266 Investigation, Manuscript submitted for publication.

267 Bell, J. L. (1996), Galileo navigation team file release: Final updated ephemeris file for probe
268 reconstruction JPL Doc. [960730-OD126], Jet Propul. Lab., Pasadena,Calif.,
269 http://naif.jpl.nasa.gov/pub/naif/GLL/kernels/spk/s960730a.bsp.lbl.

270 Bolton, S.J., R.M. Thorne, S. Bourdarie, I. DePater, and B. Mauk (2004), in Jupiter, The Planet,
271 Satellites and Magnetosphere, ed. By F. Bagenal, T.E. Dowling, and W.B. McKinnon
272 (Cambridge University Press, Cambridge), 674-676.

273 Bolton, S.J., A. Adriani, V. Adumitroaie, J. Anderson, S. Atreya, J. Bloxham, S. Brown, J. E.P.
274 Connerney, E. DeJong, W. Folkner, D. Gautier, S. Gulkis, T. Guillot, C. Hansen, W.B.
275 Hubbard, L. Iess, A. Ingersoll, M. Janssen, J. Jorgensen, Y. Kaspi, S. M. Levin, C. Li, J.
276 Lunine, Y. Miguel, G. Orton, T. Owen, M. Ravine, E. Smith, P. Steffes, E. Stone, D.
277 Stevenson, R. Thorne, and J. Waite (2017), Jupiter's interior and deep atmosphere: the
278 first close polar pass with the Juno spacecraft, Manuscript submitted for publication.

279 Carr, T.D., M.D. Desch, and J.K. Alexander (1983), in Physics of the Jovian Magnetosphere, ed.
280 A.J. Dessler, Cambridge University Press, 226-284.

281 Connerney, J. E. P., M. H. Acuña, N. F. Ness (1981), Modeling the jovian current sheet and
282 inner magnetosphere, J. Geophys. Res., 86, 8370-8384.

283 Connerney, J. E. P., M. H. Acuña, N. F. Ness, and T. Satoh (1998), New models of Jupiter's
284 magnetic field constrained by the Io flux tube footprint, J. Geophys. Res., 103(A6),
285 11929–11939, doi:10.1029/97JA03726.

286 Connerney, J. E. P., M. Benn, J. B. Bjarno, T. Denver, J. Espley, J. L. Jorgensen, P. S. Jorgensen,
287 P. Lawton, A. Malinnikova, J. M. Merayo, S. Murphy, J. Odom, R. Oliversen, R.
288 Schnurr, D. Sheppard, E. J. Smith, (2017) The Juno Magnetic Field Investigation, Space
289 Sci. Revs., doi: 10.1007/s11214-017-0334-z

290 Divine, N., and H.B. Garrett (1983), J. Geophys. Res. 88, 6889–6903.

291 Fillius, W. (1976), The trapped radiation belts of Jupiter, in Jupiter, T. Gehrels (ed), University
292 of Arizona Press, 896-927.

293 Fischer, H. M., E. Pehlke, G. Wibberenz, L.J. Lanzerotti, and J.D. Mihalov (1996), High-energy
294 charged particles in the innermost jovian magnetosphere, Science, 272, 856-858.

295 Garrett, H.B., I. Jun, J.M. Ratliff, R.W. Evans, G.A. Clough, and R.W. McEntire (2003), Galileo
296 Interim Radiation Electron Model, (The Jet Propulsion Laboratory, California Inst. of
297 Technology, Pasadena, CA), JPL Publication 03-006, 72 pages.

298 Garrett, H.B., S.M. Levin, S.J. Bolton, R.W. Evans, and B. Bhattacharya (2005), Geophys. Res.
299 Lett. 32(4), L04104, doi:10.1029/2004GL021986.

300 Mauk, B.H., Haggerty, D.K., Jaskulek, S.E. et al. (2014), The Jupiter Energetic Particle Detector
301 303 Instrument (JEDI) Investigation for the Juno Mission, Space Sci Rev, 304
302 doi:10.1007/s11214-013-0025-3.

303 Mauk, B.H., D. K. Haggerty, C. P. Paranicas et al. (2016), Juno observations of energetic
304 charged particles over Jupiter's polar regions: Analysis of mono-1 and bi-directional
305 electron beams, Geophys. Res. Lett., submitted, this issue.

306 Santos-Costa, D. and S.J. Bolton (2008), Planet. Space Sci., 56, 326.

307 Santos-Costa, D., I. de Pater, R. J. Sault, M. A. Janssen, S. M. Levin and S. J. Bolton (2014),
308 A&A 568, A61, doi:10.1051/0004-6361/201423896.